

# Perceived risk determines spatial position in fish shoals through altered rules of interaction

Andreu Puy,<sup>1,\*</sup> Elisabet Gimeno,<sup>1,2</sup> Francesc S. Beltran,<sup>3</sup> Ruth Dolado,<sup>3</sup> M.  
Carmen Miguel,<sup>2,4</sup> Christos C. Ioannou,<sup>5</sup> and Romualdo Pastor-Satorras<sup>1</sup>

<sup>1</sup>*Departament de Física, Universitat Politècnica de Catalunya, Campus Nord B4, 08034 Barcelona, Spain*

<sup>2</sup>*Departament de Física de la Matèria Condensada,  
Universitat de Barcelona, Martí i Franquès 1, 08028 Barcelona, Spain*

<sup>3</sup>*Departament de Psicologia Social i Psicologia Quantitativa,  
Universitat de Barcelona, Passeig Vall d'Hebron, 171, Barcelona 08035, Spain*

<sup>4</sup>*Institute of Complex System (UBICS), Universitat de Barcelona, Barcelona 08028, Spain*

<sup>5</sup>*University of Bristol, School of Biological Sciences,  
Life Sciences Building, 24 Tyndall Avenue, Bristol BS8 1TQ, UK*

(Dated: October 15, 2024)

Risk perception plays a key role in shaping the collective behavior of moving animal groups, yet the effects of variation in perceived risk within groups is unknown. Here, we merge two subgroups of fish with different levels of perceived risk, manipulated through habituation to the experimental arena, and quantitatively analyze their movement. Fish with heightened risk perception tend to occupy more central positions within the group, consistent with the selfish herd hypothesis. This behavior appears to be driven by adjusted local interactions with nearby individuals. Compared to more habituated fish, these individuals also exhibit greater coordination, shorter burst-and-coast dynamics, more efficient information transmission, and a stronger tendency to adopt follower roles. To validate the findings, we develop a machine learning tool that successfully classifies the subgroup identity of individual fish. Our study demonstrates how differences in local-scale inter-individual interactions can drive spatial assortment within groups, based on heterogeneity in the perception of risk.

Flocks of birds and schools of fish can move with such cohesion and coordination that they appear to act with a single ‘collective mind’ [1]. This can give the impression that individuals within the group are homogeneous, including in the behaviors that they use to interact with others in the group. However, variation between individuals within animal groups is the rule rather than the exception [2], and variation forms the bedrock upon which evolutionary selection can act to shape the traits that determine collective behavior [3]. The variation between individuals within groups that can impact collective behaviour varies widely from traits that are fixed within the lifetime of an individual such as sex, to those that vary slowly over time such as age, and those that can change within seconds, such as the perception of predation risk [2].

Collective behavior is known to be impacted by the level of predation risk perceived by group members. The extent to which individuals perceive their environment to be risky depends on their evolutionary history and early-life experience [4], recent or current cues that indicate risk [5], and familiarity with their environment [6]. An increased perception of predation risk increases group size and cohesion, which is consistent with multiple mechanisms that reduce the rate and success of attacks from predators [7, 8], and is also expected from Hamilton’s 1971 selfish herd hypothesis [9], where individuals reduce the distance to their near neighbors to minimize their

‘domain of danger’, i.e. the space around them that is closer to themselves than any other potential target. Individuals can also rely more on social information [10] and become more responsive to one another when the perception of risk is greater [11].

Heterogeneity between individuals in their perception of risk can generate non-random spatial structure within groups, known as assortment. Some spatial positions are associated with a greater risk of predation, usually the front and periphery of the group, but these positions also allow a greater access to food resources [12]. This is supported by bolder individuals, i.e. those with a consistently lower perception of risk, tending to be at the front of moving groups [13], as well as larger individuals that are less at risk from predators [14]. Non-random assortment within groups has also been demonstrated with informational state, e.g. the extent to which individuals are experienced with their environment [15, 16]. However, in all of these studies, variation between individuals was unmanipulated and often correlated to other traits including body size, age and reproductive status, thus a direct effect of differences in informational state, including in the perceived level of risk, on spatial position has not been demonstrated.

Research suggests that in most species of fish and birds that form highly coordinated, cohesive and dynamic groups, this behavior is achieved through rapid responses to passive cues of neighbors changing their speed and direction, rather than active signals such as alarm calls [3]. These are commonly explained from simple interactions arising from decision making processes of individuals. A

---

\* [andreu.puy@upc.edu](mailto:andreu.puy@upc.edu)

standard framework to study these interactions is based on the concept of effective forces acting on individuals. Social forces arise from interactions among group members and are typically described by a combination of attraction, repulsion, and alignment [17–19]. Attraction brings individuals together into groups, repulsion prevents collisions, and alignment ensures individuals move in the same direction as their neighbors. Furthermore, interactions between pairs can be asymmetric and non-reciprocal [20], leading to a net information flow with leader-follower relationships [21].

Previous studies have explored how risk perception affects collective behavior, how pre-existing differences between individuals in risk perception result in spatial assortment within groups, and the fine-scale ‘rules of interaction’ that underpin collective behavior [22]. Here, we instead manipulated the informational state of individuals within fish shoals, testing whether fish with a reduced perception of risk (from habituation to the test environment) occupied different spatial positions when shoaling with non-habituated individuals with a greater risk perception. Such a design where groups consist of individuals that vary in their experience is representative of fission-fusion dynamics, frequently observed in fish [23], where group membership is fluid and groups merge and split. Importantly, experimentally manipulating the perceived risk of individuals allows us to test for the effects of inter-individual variation in isolation, thus minimizing confounding effects, unlike studies that rely on pre-existing sources of inter-individual variation. Through detailed analysis of the fish’s responses to other fish, we then demonstrate the differences in interaction rules, coordination, leader-follower behavior, and individual self-propulsion forces between habituated and non-habituated fish, and how local-scale individual behaviors can result in global-scale patterns of spatial assortment as predicted from an influential model of collective motion [24]. We also investigate the temporal evolution of interactions throughout the two-hour duration of the experiment. Finally, to conclusively demonstrate behavioral differences, we develop a machine learning tool to classify individuals into their respective subgroups based on their observed behaviors.

We used black neon tetras (*Hyphessobrycon herbertaxelrodi*), a highly social fish species that forms polarized, compact, and planar schools. Sixteen individuals, already familiar with each other, were divided into two subgroups of eight individuals, designated as *habituated* (Hab) and *non-habituated* (Non-hab). The habituated subgroup underwent a habituation process in an experimental tank with an approximately two-dimensional setting, where individuals swam freely for two hours each day over five days. In contrast, the non-habituated subgroup was not exposed to the experimental tank. On the sixth day, both subgroups were merged in the experimental tank, and their individual trajectories were recorded as they swam freely for two hours. The experiment was replicated three times with different sets of individuals,

labeled series A, B, and C. Supplementary Video S1 provides a sample of the school’s behavior, with digitized trajectories overlaid on to the video.

## RESULTS

### Group-level spatial interactions

We initially tested whether the subgroup with a greater perception of risk (the individuals not habituated to the environment) occupied different spatial positions within the group compared to habituated individuals. We thus examined the spatial density distribution of individuals based on their normalized relative positions within the group,  $(\vec{r}_i - \vec{r}_{CM})/R_g$ . Here,  $\vec{r}_i \equiv (x_i, y_i)$  denotes the positions of the individuals,  $\vec{r}_{CM} \equiv \frac{1}{N} \sum_i \vec{r}_i$  represents the position of the center of mass CM of a group with  $N$  individuals, and  $R_g \equiv \sqrt{\frac{1}{N} \sum_i |\vec{r}_i - \vec{r}_{CM}|^2}$  is the radius of gyration, indicating the typical length scale of the group. Consistent with the selfish-herd hypothesis, non-habituated individuals occupy peripheral positions less frequently than habituated individuals (Fig. 1a). This is robust across the different series (Supplementary Figs. S1a-c) and remains consistent throughout the two-hour duration of the experiment (Supplementary Figs. S2a and b).

This analysis can be further refined by separating it into the  $x$  and  $y$ -coordinates. In both axes, the center of the group is dominated by non-habituated individuals (Figs. 1b and c; Supplementary Figs. S1d-i for different series). However, while in the  $x$ -coordinate distributions are symmetric, we find that in the  $y$ -coordinate (oriented along the direction of the center-of-mass velocity,  $\vec{v}_{CM} = \frac{1}{N} \sum_i \vec{v}_i$ ), habituated individuals tend to be positioned more towards the front of the group (positive  $y_i - y_{CM}$  values), consistent with frontal positions being perceived as riskier [12].

The selfish herd hypothesis also predicts that individuals will dynamically change their spatial positions to avoid being on the periphery (i.e. border) of the group. We define an individual is on the border at a given frame if it belongs to the convex hull of the group, which is the smallest convex polygon that contains all individuals. With this definition, we have, on average, 7.2 individuals on the border and 8.8 individuals in the inner part of the group at any given frame (Supplementary Fig. S3a). Consistent with our previous results, there were more habituated individuals on the border (4.0 on average) than non-habituated individuals (3.2 on average) (Supplementary Fig. S3b). Fig. 1d shows the PDF of the duration time on the border  $\Delta t_{\text{border}}$  for individuals in each subgroup, defined as the time that an individual spends on the border, i.e. between when it enters and leaves the convex hull. For short duration times (below 5 seconds), individuals in both subgroups exhibit similar behavior, with a characteristic duration time around 0.15 s. How-

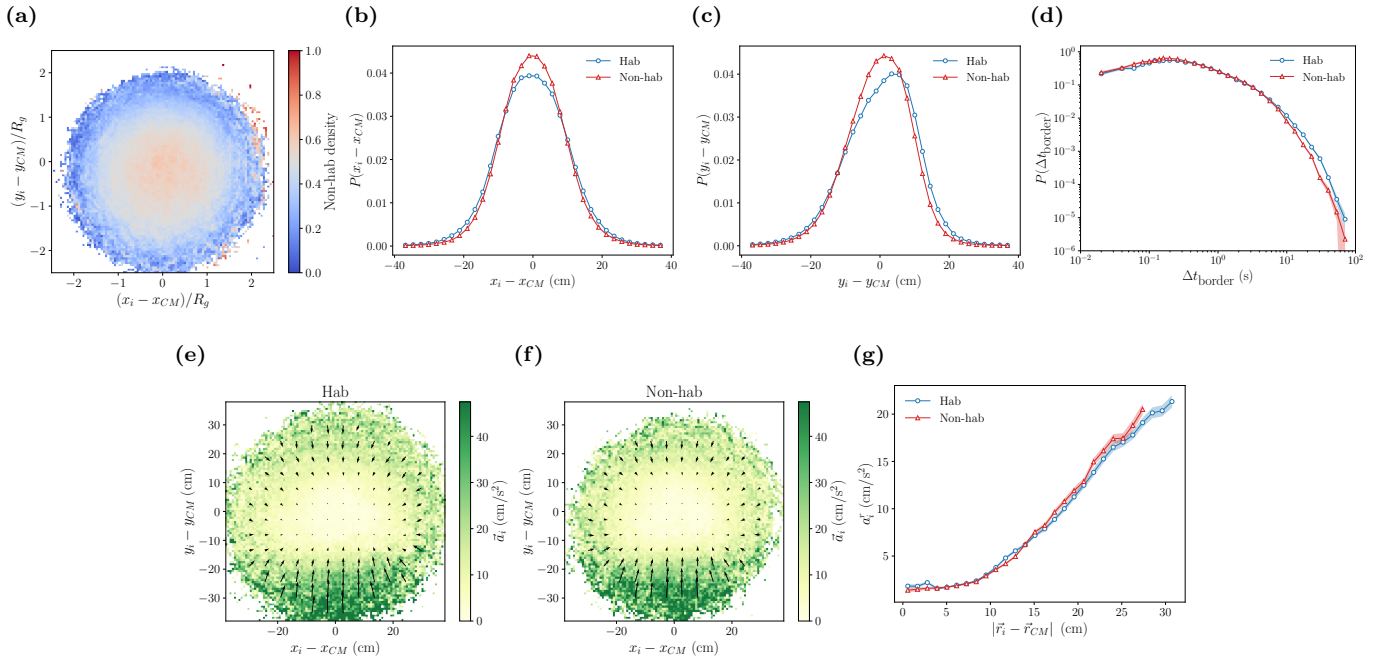


FIG. 1. Group-level spatial interactions. (a) Spatial density distribution of non-habituated individuals  $i$  relative to the center of mass CM,  $(\vec{r}_i - \vec{r}_{CM})/R_g$ . It is calculated by normalizing the counts of non-habituated individuals against the counts of all individuals across all time frames for all series. The  $y$ -coordinate is oriented along the direction of motion of the group given by the center-of-mass velocity  $\vec{v}_{CM} \equiv \frac{1}{N} \sum_i \vec{v}_i$ . (b) and (c) Probability density functions (PDFs) of the relative position of individuals with respect to the center of mass,  $\vec{r}_i - \vec{r}_{CM}$ , along the (b)  $x$ -coordinate and (c)  $y$ -coordinate. (d) PDF of the duration time of individuals on the border of the group  $\Delta t_{\text{border}}$ . (e) and (f) Average acceleration (force map) depending on the relative position with respect to the center of mass,  $\vec{r}_i - \vec{r}_{CM}$ , for (e) habituated and (f) non-habituated individuals. The force components are displayed with arrows and the modulus with the colormap. (g) Average modulus of the acceleration in the radial direction of the force map,  $a_i^r$ , depending on the distance to the center-of-mass,  $|\vec{r}_i - \vec{r}_{CM}|$ . In all 2-dimensional plots we have excluded bins with fewer than 15 counts to reduce statistical noise. For all PDFs we show error bands calculated from the standard deviation of a Bernoulli distribution, with the probability given by the fraction of counts in each bin. In (g) we show error bands given by the standard deviation of the mean.

ever, for longer duration times, non-habituated individuals tend to spend less time on the border compared to habituated individuals (also see Supplementary Fig. S1j-l). Additionally, while the qualitative behavior stays the same across time, at later times in the experiments, individuals in both subgroups tend to spend longer intervals on the border (Supplementary Fig. S2e).

To infer effective forces acting on individuals based on their spatial position within the group, we use the force map method [20, 25, 26]. This infers forces from the dependency of the acceleration with some relevant variables, while averaging over other variables (see Methods). Despite the differences in spatial position between habituated and non-habituated fish, we find the force maps for habituated (Fig. 1e) and non-habituated (Fig. 1f) individuals are very similar, with no net force for central regions of the group and arrows pointing inwards at larger distances, signaling an attractive force towards the centre. This effective force is responsible for individuals forming cohesive groups. Additionally, we find forces are stronger for individuals at the rear of the group (negative  $y$ -values). These results are consistent across experimen-

tal series (Supplementary Figs. S1m-o).

To take a more detailed view of the trends in the force maps, we present the average modulus of the acceleration in the radial direction of the force map,  $a_i^r$ , as a function of the distance to the center-of-mass,  $|\vec{r}_i - \vec{r}_{CM}|$  (Fig. 1g and Supplementary Figs. S1p-r). Non-habituated individuals show slightly stronger attractive forces at further distances from the group centre, which is coherent with their greater tendency to occupy the central regions of the group. Furthermore, attractive forces decrease over time (Supplementary Fig. S2f). This is consistent with the temporal trend that the size occupied by the group expands (Supplementary Fig. S2c and d), i.e. the group becomes less cohesive as time progresses, consistent with previous work [6].

### Local-level spatial interactions

Group-level behaviors, such as spatial positioning, are typically understood to arise from the superposition of local interactions between individuals. In this section,

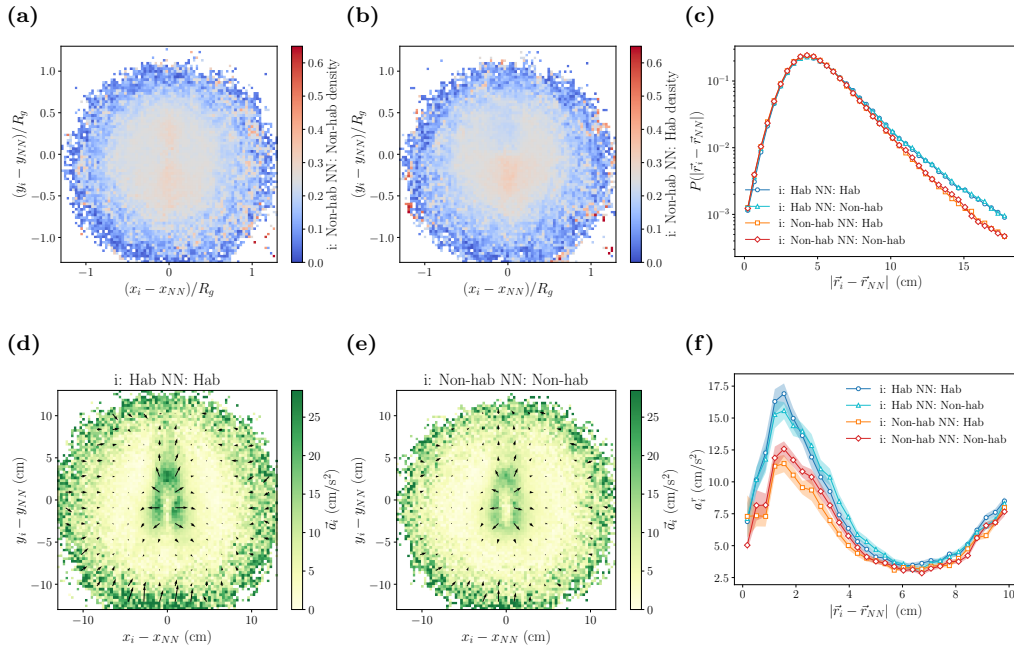


FIG. 2. Local-level spatial interactions. Spatial density distribution of non-habituated individuals  $i$  with either (a) non-habituated or (b) habituated nearest neighbors  $NN$  as a function of their normalized relative positions  $(\vec{r}_i - \vec{r}_{NN})/R_g$ . The  $y$ -coordinate is oriented along the direction of motion of individual  $i$ . (c) PDFs of the distance between the individual  $i$  and its nearest neighbor  $NN$ ,  $|\vec{r}_i - \vec{r}_{NN}|$ . Average acceleration (attraction-repulsion force map) of individual  $i$  depending on its relative position to its nearest neighbor  $NN$ ,  $\vec{r}_i - \vec{r}_{NN}$ , for both (d) habituated and (e) non-habituated pairs. (f) Average modulus of the acceleration in the radial direction of the attraction-repulsion force map,  $a_i^r$ , depending on the distance to the nearest neighbor,  $|\vec{r}_i - \vec{r}_{NN}|$ .

we study local-level spatial interactions between individuals and their nearest neighbors. We analyze behavioral differences depending on both the individual's subgroup identity and the nearest-neighbor's subgroup identity, to determine whether individuals can recognize and respond differently to these identities.

We first analyze the spatial density distribution of individuals depending on their normalized relative positions with respect to their nearest neighbor  $NN$ ,  $(\vec{r}_i - \vec{r}_{NN})/R_g$ . The results support the selfish herd hypothesis at the local level, with non-habituated individuals positioning themselves closer to their nearest neighbors than habituated individuals (Figs. 2a and b). We find a slight difference in the central regions of the density distributions for different subgroup identities: non-habituated individuals tend to be located behind habituated nearest neighbors. These findings are robust for complementary plots with habituated individuals (Supplementary Fig. S4), across series (Supplementary Figs. S5a-f) and constant across the 2 hour duration of the experiment (Supplementary Figs. S6a-d).

To better quantify local-level spatial interactions, Fig. 2c (Supplementary Figs. S5g-i for different series) shows the PDF of the distances between individuals and their nearest neighbors. The peak of the PDF, indicating the preferred nearest-neighbor distance, is identical for all individuals and neighbors. However, there are

fewer non-habituated individuals at the longer distances, regardless of the nearest neighbor identity. Over time, nearest-neighbor distances tend to increase (Supplementary Figs. S6e).

We infer effective spatial forces at the local level with the attraction-repulsion force map [20, 25, 26], which extracts attraction-repulsion forces from the average individual acceleration  $\vec{a}_i$  based on the relative position of nearest neighbors,  $\vec{r}_i - \vec{r}_{NN}$ . The force maps (Figs. 2d and e) for interactions between habituated and non-habituated individuals are qualitatively similar: for near distances arrows point outward, indicating the focal individual experiences a repulsive force away from the neighbor; for intermediate distances, there is an area with no net force (the equilibrium distance); and for longer distances, arrows point inward, signaling an attractive force toward the neighbor. However, the repulsive force between non-habituated individuals appears weaker than for habituated individuals, which helps explain the observed patterns in the spatial density distributions. To quantify this difference, we also analyze the average modulus of the acceleration in the radial direction of the force map,  $a_i^r$  as a function of the distance to the nearest neighbor,  $|\vec{r}_i - \vec{r}_{NN}|$  (Fig. 2f). We find that the peak for small nearest-neighbor distances, associated with the repulsive forces, is considerably lower for non-habituated individuals compared to habituated individuals, regardless of

the subgroup identity of the nearest neighbor. In contrast, their behaviors are similar within the equilibrium distance and attractive regions. These results are robust across different series (Supplementary Fig. S5j-l). Across time, repulsive forces increase, the equilibrium distance expands, and attractive forces decrease (Supplementary Fig. S6f).

### Group-level coordination

In this section, we aim to study the speed and orientation of individuals relative to the school. We begin by examining the modulus of the velocity differences between the individual and the group,  $|\vec{v}_i - \vec{v}_{CM}|$ . We find velocities of non-habituated fish are more aligned with the average group motion (Fig. 3a). Similarly, we analyze the polarization  $\phi$  [27] of the subgroup,

$$\phi \equiv \left| \frac{1}{N_s} \sum_i \frac{\vec{v}_i}{v_i} \right|,$$

where we sum over the  $N_s$  individuals of the subgroup. Polarization approaches 1 if the subgroup is ordered and aligned, with all individuals moving in the same direction, and it approaches 0 if the subgroup is disordered, with individuals moving in random and independent directions. Non-habituated individuals exhibit slightly larger polarization values (Fig. 3b), indicating they are more aligned with each other than habituated individuals. Both measures are consistent for different series (Supplementary Figs. S7a-f). Additionally, over time, the modulus of the velocity differences increases (Supplementary Fig. S8a), and polarization decreases (Supplementary Fig. S8b), indicating that alignment with the group decreases over time, again consistent with previous work on fish shoals [6].

According to the selfish herd hypothesis, individuals perceiving higher risk may orient themselves towards the center of the group to reach the safer central positions. This can be quantified as the orientation of individuals with respect to the group,

$$\theta_{i,CM} = \arctan \left( \frac{(\vec{r}_{CM} - \vec{r}_i) \times \vec{v}_i}{(\vec{r}_{CM} - \vec{r}_i) \cdot \vec{v}_i} \right),$$

where an individual pointing directly towards the center of mass has  $\theta_{i,CM} = 0$ , while an individual pointing directly away from the center of mass has  $|\theta_{i,CM}| = \pi$  (Supplemental Fig. S9). Despite only a few individuals tending to point towards the center, these are more likely to be non-habituated rather than habituated individuals (Fig 3c, Supplementary Figs. S7g-i). Differences between the subgroups tend to decrease over time, but they still remain noticeable at the end of our two-hour recordings (Supplementary Fig. S8c).

### Local-level coordination

In addition to coordination with the group and subgroup, coordination can also be quantified at a local level using relative velocities. The probability distribution of relative velocities between non-habituated individuals and their non-habituated nearest neighbors (Fig. 4a) tends to cluster in the central region of the plot, reflecting lower velocity differences compared to other types of neighbor pairs. In contrast, non-habituated individuals with habituated nearest neighbors (Fig. 4b) are more frequently located in the half-bottom region of the plot, i.e. they tend to be slower than habituated fish. The findings are consistent for complementary plots with habituated individuals (Supplementary Fig. S10), across series (Supplementary Figs. S11a-f) and over time (Supplementary Figs. S12a-d).

Fig. 4c shows the probability density of velocity differences for the four subgroup combinations of nearest-neighbor pairs (also see Supplementary Figs. S11g-i). Velocity differences are lower among non-habituated pairs, indicating higher alignment at the local level, compared to habituated pairs. Mixed pairings, involving habituated individuals and non-habituated nearest neighbors, fall in between. Additionally, we observe that over time, velocity differences increase, corresponding to a decrease in local alignment (Supplementary Fig. S12e).

To interpret these patterns, we infer the effective local alignment forces using the alignment force map [20]. This map shows the average acceleration of individuals,  $\vec{a}_i$ , as a function of their relative velocities with respect to their nearest neighbors,  $\vec{v}_i - \vec{v}_{NN}$  (Supplementary Fig. S13). There is qualitatively similar behavior for both subgroups, i.e. in both cases we observe a selective alignment mechanism with faster nearest neighbors, as described in Ref. [20]. Notably, non-habituated individuals with habituated nearest neighbors occupy with higher probability the region in the velocity density distribution (Fig. 4b) that corresponds to effective alignment interactions, characterized by inward-pointing arrows. In contrast, habituated individuals with non-habituated nearest neighbors are more likely to occupy areas of the plot characteristic of apparent anti-alignment interactions (Supplementary Fig. S10b), with outward-pointing arrows. These regions and effective interactions can be rationalized in terms of leader-follower relationships [20].

### Leader-follower relationships

Information flow is naturally observed from individuals at the front of a group to those behind [28, 29], and from individuals moving at higher speeds to those with lower velocities [20, 30]. This implies that non-habituated individuals, tending to position themselves in the rear of the group and exhibiting lower velocities compared to their habituated nearest neighbors, may be following habitu-

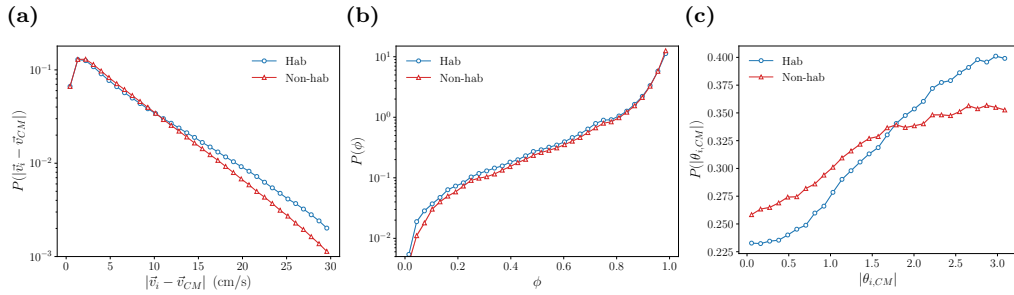


FIG. 3. Group-level coordination. PDFs of (a) the modulus of the velocity differences between individuals and the center of mass,  $|\vec{v}_i - \vec{v}_{CM}|$ , (b) the polarization  $\phi$  and (c) of the absolute value of the individuals' orientation relative to the CM,  $\theta_{i,CM}$ .

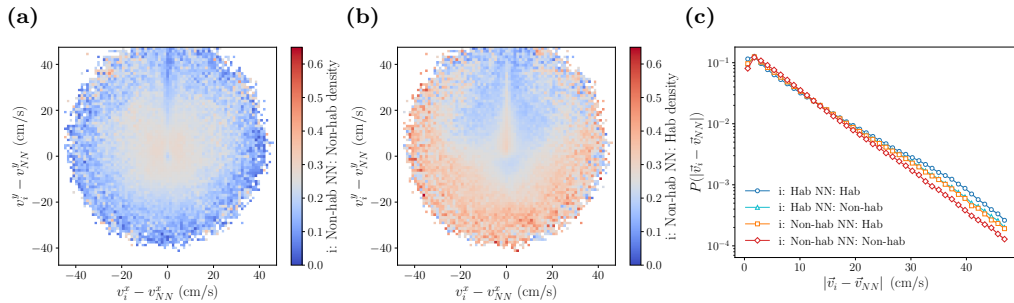


FIG. 4. Local-level coordination. Velocity density distribution of non-habituated individuals  $i$  with (a) non-habituated and (b) habituated nearest neighbors  $NN$  depending on their relative velocities  $\vec{v}_i - \vec{v}_{NN}$ . The  $y$ -coordinate is oriented along the direction of motion of individual  $i$ . (c) PDFs of the modulus of the relative velocity  $|\vec{v}_i - \vec{v}_{NN}|$ .

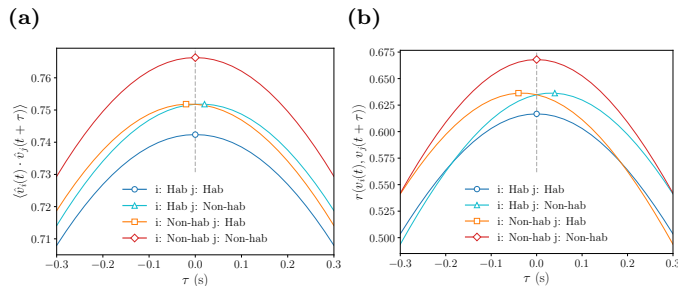


FIG. 5. Leader-follower relationships. Correlations in (a) the orientation and (b) the speed (Pearson correlation coefficient  $r$ ) between an individual  $i$  and an individual  $j$  at a delayed time  $\tau$ . The markers denote the maximum of each line, while the vertical dashed line represents  $\tau = 0$ . Correlation values range from  $[-1, 1]$ . If there are leader-follower interactions, a follower requires some time to react and copy the leader. This results in correlations having a higher value at that delayed time, provided the sampling interval (here, the frame rate of the video) is higher than the reaction time of the follower. If the maximum occurs for a positive delay  $\tau$ , this implies individual  $i$  is the leader with respect to individual  $j$ . While for a negative delay, individual  $i$  is the follower. Additionally, the value of the maximum reflects the amount of information transmitted by the leadership flow.

ated individuals. To explicitly test this, we analyze the transmission of information between pairs of individuals and determine leader-follower relationships.

We employ correlations between an individual  $i$  and an individual  $j$  at a delayed time  $\tau$  and average them across all time frames  $t$  maintaining the subgroup identities of individuals. We consider two types of correlations, in the orientation given by  $\langle \hat{v}_i(t) \cdot \hat{v}_j(t + \tau) \rangle$  [28] (Fig. 5a)

and in the speed given by the Pearson correlation coefficient  $r(v_i(t), v_j(t + \tau))$  [20, 25] (Fig. 5b). When considering non-habituated individuals with respect to habituated individuals, both correlations have their maxima at negative delays  $\tau$  (Fig. 5), confirming that non-habituated individuals behave as followers. Conversely, habituated individuals exhibit maximum correlations at positive delays with respect to non-habituated individu-

als, indicating they act as leaders. Additionally, the maximum correlation between pairs of non-habituated individuals is higher than between pairs of habituated individuals, implying that non-habituated individuals transmit information of orientations and speeds more effectively among themselves. Mixed pairs of habituated and non-habituated individuals show intermediate levels of information transmission. These trends tend to be robust across different series (Supplementary Fig. S14). Over time, correlations decrease, indicating a reduction in the transmission of information, again consistent with previous work [6]. Moreover, in the case of orientation correlations, we observe a switch in leader-follower roles between habituated and non-habituated individuals during the last half hour (Supplementary Fig. S15a).

### Burst-and-coast dynamics

Apart from social interactions, we can examine individual behavior by studying differences in self-propulsion forces between the two subgroups. Many fish species exhibit oscillations in speed due to a burst-and-coast mechanism [31–33] (Fig. 6a), where increased speed is associated with an active phase powered by the fish muscles and speed decreases with a passive gliding phase. Fish with different perception of risk may adapt their burst-and-coast mechanism accordingly, as has been shown when comparing fish from high versus low predation environments when tested in a collective decision making assay [34].

Both subgroups exhibit the same qualitative bimodal behavior in the PDF of individual speeds  $v_i$  (Fig. 6b), with a large narrow peak at small speeds ( $v \sim 3$  cm/s) corresponding to the minimum of the burst-and-coast dynamics, and a smaller, broader peak or shoulder at large speeds ( $v \sim 35$  cm/s) corresponding to the maximum of the burst-and-coast dynamics (Fig. 6a). The large speed peak is broader because the maximum of the burst-and-coast dynamics exhibits more variability. However, non-habituated fish exhibit their two peaks at intermediate speeds compared to habituated individuals, indicating a constrained burst-and-coast movement, with a higher minimum speed and a lower maximum speed. This is consistent across different series (Supplementary Figs. S16a-c). Additionally, we observe that speeds decrease over time (Supplementary Fig. S17a).

To quantify the burst-and-coast dynamics in more detail, we consider the time interval  $\Delta t_{BC}$  and the speed variability  $\Delta v_{BC}$  between consecutive minima. We define speed variability as  $\Delta v_{BC} \equiv \Delta v_{\text{up}} + \Delta v_{\text{down}}$ , where  $\Delta v_{\text{up}}$  and  $\Delta v_{\text{down}}$  are the absolute value of the speed increments during the increase and decrease phases of the burst-and-coast dynamics, respectively. We find that non-habituated individuals, compared to habituated individuals, exhibit shorter burst-and-coast dynamics, characterized by shorter time intervals  $\Delta t_{BC}$  and lower speed variabilities  $\Delta v_{BC}$  (Figs. 6c and d and Sup-

plementary Figs. S16d-i). Over time, individuals tend to stretch their burst-and-coast motion, resulting in longer time intervals and greater speed variabilities (Supplementary Figs. S17b and c).

### Machine learning identification tool

In the previous sections, we identified distinct aggregated behaviors and interactions among individuals from subgroups that vary in their perceived level of risk. To further confirm these differences and quantify the most prominent ones, we now develop a machine learning tool to classify individuals by their subgroup identity. Our goal is to maximize the accuracy of predicting the correct subgroup identity of individuals based on observables recorded in two scenarios: at a given instant of time and over a temporal window.

In machine learning, the task of classifying data into categories belongs to the class of supervised learning methods. It consists of building a model from a dataset to predict an output label based on input variables or features. The model is initially fitted on a training dataset, and its performance is then evaluated using a separate test dataset. To ensure robustness, we employ cross-validation, where the performance is averaged across different random splits of the dataset. Among the many classification algorithms available, we choose the regularized gradient boosting implemented by the XGBoost library [35] due to its strong predictive performance, as evidenced by its success in numerous machine learning competitions. We also tested a logistic regression algorithm, but XGBoost yielded superior results.

For the first scenario, we take a snapshot of the individuals at a given instant and attempt to predict their subgroup identities. We include variables analyzed in previous sections as features (see [Methods](#)). Additionally, we reduced temporal correlations in the dataset by using samples taken every 100 frames (corresponding to 2-second intervals; see [36]). The performance of the instantaneous machine learning tool is shown in the confusion matrix in Table Ia. The confusion matrix displays the probability of correctly predicting the subgroup identity of an individual based on its true identity. We find that the instantaneous machine learning tool achieves a modest accuracy, approximately 3.5% above random guessing. This indicates that identifying individuals' subgroup identities based solely on their instantaneous behavior and interactions is challenging. Additionally, XGBoost quantifies the importance of the features used in the fitted model. In particular, we analyzed the total number of times a feature is used to split the data across all trees normalized against all features. We find the different features used share comparable weights (Supplementary Fig. S18a).

In our second scenario, we observe individuals over a 10-minute time window before predicting their subgroup identities. To aggregate results across the window, we bin

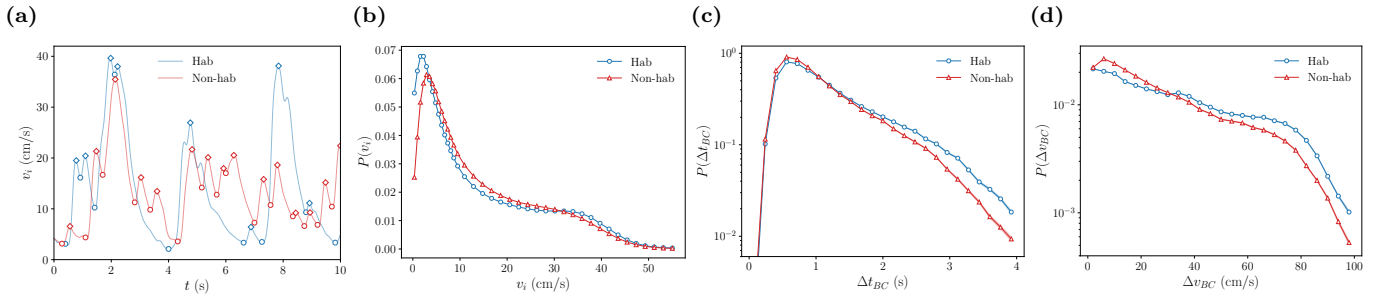


FIG. 6. Burst-and-coast dynamics. (a) Temporal evolution of the speed for a single habituated and non-habituated individual for a time interval of 10 s in series A. Local maxima and minima are marked with diamonds and circles, respectively. PDFs of (b) the individuals speeds  $v_i$ , (c) the time interval  $\Delta t_{BC}$  and (d) the speed variability  $\Delta v_{BC}$  between consecutive minima in the burst-and-coast oscillations of speeds.

TABLE I. Confusion matrices with the prediction performance of (a) the instantaneous and (b) the temporal window machine learning tools. Results are averaged across (a) 4 folds and (b) 30 folds with cross-validation.

		Predicted	
		Hab	Non-hab
True	Hab	0.536(5)	0.464(5)
	Non-hab	0.466(3)	0.534(3)

		Predicted	
		Hab	Non-hab
True	Hab	0.77(3)	0.23(3)
	Non-hab	0.21(2)	0.79(2)

variables into histograms. We use the bin values as features for the machine learning model, as well as measures of maximum leader-follower correlations (see [Methods](#)). This machine learning identification tool achieves a substantial accuracy of nearly 80% in predicting the correct subgroup identities of individuals, confirming objective behavioral differences among individuals (Table Ib). We also rank features by their weight as provided by XGBoost (Supplementary Figs. S18b and S19), which indicate that features associated with histogram maxima, as well as measures of maximum leader-follower correlations, tend to have greater importance.

## DISCUSSION

Our comprehensive, large-scale dataset, combined with techniques to extract effective interactions, enabled us to conduct a quantitative analysis of how differences in perceived risk within groups affects behaviour. We provide

evidence that fish adapt their behavior based on their perceived level of risk, depending on the extent of habituation, but also the temporal evolution within the experimental trials, which showed trends consistent with previous work [6]. These adaptations manifested at both the group and local levels in terms of spatial position and velocity coordination, leader-follower relationships, and individual self-propulsion forces. While interactions of individuals evolved over time, the distinct behaviors of the subgroups remained consistent throughout the two-hour experiment. We conclusively verified and analyzed interactions by building a machine learning tool that identifies the subgroup identity of individuals.

By combining analyses of the spatial positioning of the habituated and non-habituated fish with analyses quantifying the interactions between individuals, we are able to demonstrate how individuals with a greater perception of risk tend to occupy central positions. Despite the influence of the selfish herd hypothesis [9], the movement rules that individuals use to achieve the selfish herd effect remain debated [37, 38], and this line of research has largely been independent of research in collective behaviour on the rules of interactions within animal groups [19]. The selfish herd hypothesis has been supported by several studies [39–41], but recent work, especially on bird flocks, has raised questions about its validity [42, 43]. Our findings provide further support to the selfish herd effect and shed light on the interaction rules that drive this behavior. Compared to habituated individuals, non-habituated individuals show reduced repulsion to their near neighbors, and are less likely to have near neighbours further away. While we cannot discard a group-scale behaviour where individuals are attracted to the centre of the group, the small difference observed between habituated and non-habituated individuals suggest that central spatial positions are an emergent property of local-scale interactions between neighbours.

The maintenance of central spatial positions is likely to be further facilitated by non-habituated individuals being more ordered and aligned with both the group and their neighbors, and with speeds more contracted with shorter



oscillations, compared to habituated individuals. These behaviours are also likely to facilitate non-habituated individuals to follow other fish. Being led by others was suggested by non-habituated individuals occupying more rearward spatial positions within the group, and moving at lower relative speeds with respect to neighbors. Through time delays in maximum correlations of velocities with neighbors [25, 28], we confirmed that habituated individuals were leading non-habituated individuals, but also that non-habituated transmitted more effectively information about orientation and speed. This indicates that individuals with a greater perception of risk have greater reliance on social information, consistent with studies of social learning [10].

Our study was designed to manipulate the perception of risk by habituating one subgroup of individuals through repeated exposure to the test conditions, while these conditions were novel for the other subgroup. This novelty also meant that the non-habituated fish had greater uncertainty about their environment than the habituated fish, whose repeated testing provided more certain information that the test conditions were low risk. Previous studies have manipulated perceived risk with methods more likely to induce acute stress, including exposing test subjects to predators [44, 45] or alarm substances [5, 39]. Our method is less invasive and minimizes the ethical issues associated with manipulating the perception of risk, as well as being easier to implement and thus more accessible to researchers. However, future research could include a third subgroup of individuals that have greater certainty that the test conditions are high risk through exposure to predator cues.

To sum up, we have shown how differences in perceived risk within animal groups drive spatial positioning and social interactions, providing new insights into the mechanisms behind the selfish herd effect. Future work could explore the longer term dynamics where individuals on the periphery and at the front of groups alter both their informational and hunger states as they are more likely to encounter food and predators. This may generate a negative feedback that then increases their tendency to follow and occupy safer, more central positions. By introducing a novel, minimally invasive method to manipulate risk perception, we offer a potentially powerful tool for understanding group behavior dynamics with broad applications across behavioral ecology and beyond.

## METHODS

### Subjects

We employ schooling fish of the species black neon tetra (*Hyphessobrycon herbertaxelrodi*) wild-type, a small freshwater fish with a strong tendency to form cohesive, highly polarized, and planar schools [46]. Initially, 75 fish were kept in three separate main aquaria measuring  $40 \times 43 \times 30$  cm, with a sex ratio close to 1:1. From each

main aquarium, 16 fish were randomly selected, with 8 assigned to an *habituated group* and the remaining 8 to a *non-habituated group*. This resulted in 3 habituated groups and 3 non-habituated groups, comprising a total of 48 individuals (mean body length: 2.9 cm). Groups were housed in separate aquaria of identical dimensions to the main aquaria. Water conditions were maintained at  $25 \pm 2^\circ\text{C}$ , with a pH of 7.5–7.7, total hardness of  $7^\circ\text{--}10^\circ\text{dH}$ , and carbonate hardness of  $10^\circ\text{--}12^\circ\text{dH}$ , under a regular light/dark cycle. Nitrate levels were kept below 50 mg/L, while ammonia and nitrite concentrations were maintained at zero. Optimal water quality was ensured through weekly 15% water changes. The fish were fed to satiation with Ocean Nutrition Community Formula Flakes (Ocean Nutrition Europe, Belgium). Institutional guidelines for the care and use of animals were followed, and all procedures were conducted in accordance with the standards approved by the Ethics Committee of the University of Barcelona.

### Apparatus

An experimental tank measuring  $100 \times 100 \times 40$  cm and a water column with a height of 7 cm were used, allowing for approximately two-dimensional movement. Water in the experimental tank was maintained at  $24\text{--}26^\circ\text{C}$ , with the same pH and dH levels as in the aquaria. The tank was surrounded by translucent curtains made of white polyester that acted as a light diffuser and was directly lit by six lamps, providing a homogenous light intensity. Videos were recorded at 50 fps and a resolution of  $5312 \times 2988$  pixels with a digital camera (GoPro Hero 11 Black) mounted 1 m above the tank. In the recordings, the side of the tank measured 2634 pixels.

### Procedure

#### *Habituation*

Only habituated groups participated in this phase. Each group received one trial per day over 5 days. Habituation trials consisted of fish swimming freely in the experimental tank for 120 minutes. To ensure fish became acclimatized to the water in the experimental tank, prior to the habituation trial, each group was transferred from its aquarium into a bucket containing a mixture of water from the tank and the fishes' aquarium and remained there for 5 min. After the trial was completed, fish were gently captured with a net and transferred back to their aquarium, to which water from the experimental tank was added to facilitate reacclimatization. Water was then added to the experimental tank to compensate for the water transferred to the aquarium, and heaters and water filters were reintroduced for one hour to control for possible cumulative effects of the decrease in water temperature and any pheromones or chemical signals left in

the water by the preceding group.

### Test trial

On the sixth day, habituated groups were merged with the non-habituated groups of fish that came from the same main aquarium. Before starting each trial, the habituated group and the non-habituated group were transferred into different plastic containers of  $20 \times 14 \times 14$  cm each. One plastic container was placed in the upper right corner of the experimental tank and the other container in the lower right corner, the positioning of the habituated and non-habituated containers was counterbalanced between the trials. The test trial began by releasing the groups from their corresponding container and allowing the fish to swim freely in the experimental tank for 2 hours. The same procedure indicated above was repeated to acclimatize the fish before and after introducing them into the experimental tank, as well as filtering and heating the water in the experimental tank after each trial.

### Data extraction and preprocessing

Digitized individual trajectories were obtained from the video recordings using the software idtracker.ai [47]. Invalid values returned by the program caused by occlusions were corrected in a supervised way, semi-automatically interpolating with spline functions with the Validator tool of idtracker.ai. For better accuracy, we projected the trajectories in the plane of the fish movement, warping the tank walls of the image into a proper square (for more details see [20]). Moreover, we smooth the trajectories with a Gaussian filter with  $\sigma = 2$ , truncating the filter at  $5\sigma$ . Individual velocities and accelerations were obtained from the Gaussian filter using first and second derivatives of the Gaussian kernel, respectively.

We obtained 3 independent recordings of 120 minutes each (357001 frames per recording), which we labeled series A, B, and C. To mitigate spurious effects in averaging results, we discarded frames where any fish in the group remained stationary for prolonged periods. Specifically, we excluded frames where any individual moved at a speed lower than 0.95 cm/s for more than 5 seconds. This led to the removal of 0.6%, 1.0%, and 36.8% of the frames in series A, B, and C, respectively.

### Force map method

The force map method assumes a system with several force terms depending on sets of independent variables, and that the average in time of each force term is zero. Consider we want to infer a force term  $\vec{f}(x)$  as a function of only the variable  $x$ . We can achieve this from Newton's

second law by studying the acceleration depending on  $x$  while averaging over all other variables in the system,  $\vec{a}(x)$  [20, 25, 26]. Working in units of mass  $m = 1$ , Newton's second law will become  $\vec{f}(x) \simeq \vec{a}(x)$ , as all other forces will cancel out in the average. In practice, this approach is implemented by binning over the whole dataset the relevant variable  $x$  as  $\{x_k\}_{k=1,\dots,M}$ , where  $k$  is the index of the bin, and averaging the values of the acceleration on that bin,  $\vec{f}(x_k) \simeq \langle \vec{a}(x) \rangle_{x \in x_k}$ . See Ref. [20] for more information.

### Machine learning tool specifics

We employ the function `XGBClassifier` from the XGBoost python library [35], with 1000 number of boosting rounds (`n_estimators`), a 10 maximum tree depth for base learners (`max_depth`), a 0.5 boosting learning rate (`learning_rate`) and a 0.25 subsample ratio of the training instance (`subsample`). All other parameters are left on their default values.

To mitigate overfitting, we verified that each feature used independently improves the prediction accuracy and discarded other features that did not contribute to the improvement.

For the instantaneous machine learning scenario, we employ as features: the normalized relative position within the group  $(\vec{r}_i - \vec{r}_{CM})/R_g$ , the average normalized distance to other individuals  $\langle |\vec{r}_i - \vec{r}_j|/R_g \rangle$ , the relative velocity with the group  $\vec{v}_i - \vec{v}_{CM}$ , the acceleration  $\vec{a}_i$ , the speed  $v_i$ , the group velocity  $\vec{v}_{CM}$ , and the rate of change of the acceleration  $\delta \vec{a}_i \equiv \frac{d\vec{a}_i}{dt}$  (to test for possible dependencies in higher derivatives). Each component of these vectors is treated as a separate feature. The  $y$ -coordinate points in the direction of motion of the group and the individual for group and local measures, respectively.

For the 10-minute time window machine learning scenario, we use histograms for the normalized relative distance to the center of mass  $|\vec{r}_i - \vec{r}_{CM}|/R_g$ , the average normalized distance to other individuals  $\langle |\vec{r}_i - \vec{r}_j|/R_g \rangle$ , and the speed  $v_i$ . We use 20 bins in each histogram. Additionally, we include leader-follower correlations in the orientation  $\langle \hat{v}_i(t) \cdot \hat{v}_j(t + \tau) \rangle$  and in the speed  $r(v_i(t), v_j(t + \tau))$ , averaged across other individuals  $j$ . We use as features the values of these correlations for each discrete delay  $\tau$ , the delay at which the maximum correlation occurs  $\tau_i^\theta$  and  $\tau_i^v$ , and the relative difference of the maximum correlation value with respect to the group  $\Delta c_i^\theta$  and  $\Delta c_i^v$ . This relative difference is defined as  $\Delta c_i^x \equiv c_i^x - \langle c_i^x \rangle_i$ , where  $c_i^x$  is the value of the maximum, for  $x = \theta, v$ . For a visual representation of the features, see Supplementary Fig. S19.

### DATA AVAILABILITY

The experimental datasets can be accessed on Zenodo: <https://zenodo.org/records/XXX>.

- [1] I. D. Couzin, Collective cognition in animal groups, *Trends in Cognitive Sciences* **13**, 36 (2009).
- [2] J. W. Jolles, A. J. King, and S. S. Killen, The Role of Individual Heterogeneity in Collective Animal Behaviour, *Trends in Ecology & Evolution* **35**, 278 (2020).
- [3] C. C. Ioannou and K. L. Laskowski, A multi-scale review of the dynamics of collective behaviour: From rapid responses to ontogeny and evolution, *Philosophical Transactions of the Royal Society B: Biological Sciences* **378**, 20220059 (2023).
- [4] J. E. Herbert-Read, E. Rosén, A. Szorkovszky, C. C. Ioannou, B. Rogell, A. Perna, I. W. Ramnarine, A. Kotschal, N. Kolm, J. Krause, and D. J. T. Sumpter, How predation shapes the social interaction rules of shoaling fish, *Proceedings of the Royal Society B: Biological Sciences* **284**, 20171126 (2017).
- [5] M. M. G. Sosna, C. R. Twomey, J. Bak-Coleman, W. Poel, B. C. Daniels, P. Romanczuk, and I. D. Couzin, Individual and collective encoding of risk in animal groups, *Proceedings of the National Academy of Sciences* **116**, 20556 (2019).
- [6] H. E. A. MacGregor and C. C. Ioannou, Collective motion diminishes, but variation between groups emerges, through time in fish shoals, *Royal Society Open Science* **8**, 210655 (2021).
- [7] J. Krause and G. D. Ruxton, *Living in Groups* (OUP Oxford, 2002).
- [8] C. Ioannou, Grouping and Predation, in *Encyclopedia of Evolutionary Psychological Science*, edited by T. K. Shackelford and V. A. Weekes-Shackelford (Springer International Publishing, Cham, 2017) pp. 1–6.
- [9] W. Hamilton, Geometry for the selfish herd, *Journal of Theoretical Biology* **31**, 295 (1971).
- [10] M. Webster and K. Laland, Social learning strategies and predation risk: Minnows copy only when using private information would be costly, *Proceedings of the Royal Society B: Biological Sciences* **275**, 2869 (2008).
- [11] T. M. Schaerf, P. W. Dillingham, and A. J. W. Ward, The effects of external cues on individual and collective behavior of shoaling fish, *Science Advances* **3**, e1603201 (2017).
- [12] J. Krause, Differential fitness returns in relation to spatial position in groups, *Biological reviews of the Cambridge Philosophical Society* **69**, 187 (1994).
- [13] J. Balaban-Feld, W. A. Mitchell, B. P. Kotler, S. Vijayan, L. T. Tov Elem, and Z. Abramsky, Influence of predation risk on individual spatial positioning and willingness to leave a safe refuge in a social benthic fish, *Behavioral Ecology and Sociobiology* **72**, 87 (2018).
- [14] G. A. Rose, Cod spawning on a migration highway in the north-west Atlantic, *Nature* **366**, 458 (1993).
- [15] S. G. Reebs, Influence of Body Size on Leadership in Shoals of Golden Shiners, *Notemigonus crysoleucas*, *Behaviour* **138**, 797 (2001), 4535857.
- [16] L. J. N. Brent, D. W. Franks, E. A. Foster, K. C. Balcomb, M. A. Cant, and D. P. Croft, Ecological Knowledge, Leadership, and the Evolution of Menopause in Killer Whales, *Current Biology* **25**, 746 (2015).
- [17] D. J. T. Sumpter, *Collective Animal Behavior* (Princeton University Press, 2010).
- [18] T. Vicsek and A. Zafeiris, Collective motion, *Physics Reports* **517**, 71 (2012).
- [19] J. E. Herbert-Read, Understanding how animal groups achieve coordinated movement, *Journal of Experimental Biology* **219**, 2971 (2016).
- [20] A. Puy, E. Gimeno, J. Torrents, P. Bartashevich, M. C. Miguel, R. Pastor-Satorras, and P. Romanczuk, Selective social interactions and speed-induced leadership in schooling fish, *Proceedings of the National Academy of Sciences* **121**, e2309733121 (2024).
- [21] A. Zafeiris and T. Vicsek, *Why We Live in Hierarchies?: A Quantitative Treatise*, SpringerBriefs in Complexity (Springer International Publishing, Cham, 2018).
- [22] S. L. Lima and L. M. Dill, Behavioral decisions made under the risk of predation: A review and prospectus, *Canadian Journal of Zoology* **68**, 619 (1990).
- [23] C. C. Ioannou, I. D. Couzin, R. James, D. P. Croft, and J. Krause, Social organisation and information transfer in schooling fish, *Fish cognition and behavior* **2**, 217 (2011).
- [24] I. D. Couzin, J. Krause, R. James, G. D. Ruxton, and N. R. Franks, Collective Memory and Spatial Sorting in Animal Groups, *Journal of Theoretical Biology* **218**, 1 (2002).
- [25] Y. Katz, K. Tunstrom, C. C. Ioannou, C. Huepe, and I. D. Couzin, Inferring the structure and dynamics of interactions in schooling fish, *Proceedings of the National Academy of Sciences* **108**, 18720 (2011).
- [26] J. E. Herbert-Read, A. Perna, R. P. Mann, T. M. Schaerf, D. J. T. Sumpter, and A. J. W. Ward, Inferring the rules of interaction of shoaling fish, *Proceedings of the National Academy of Sciences* **108**, 18726 (2011).
- [27] T. Vicsek, A. Czirók, E. Ben-Jacob, I. Cohen, and O. Shochet, Novel Type of Phase Transition in a System of Self-Driven Particles, *Physical Review Letters* **75**, 1226 (1995).
- [28] M. Nagy, Z. Ákos, D. Biro, and T. Vicsek, Hierarchical group dynamics in pigeon flocks, *Nature* **464**, 890 (2010).
- [29] F. Romero-Ferrero, F. J. H. Heras, D. Rance, and G. G. de Polavieja, A study of transfer of information in animal collectives using deep learning tools, *Philosophical Transactions of the Royal Society B: Biological Sciences* **378**, 20220073 (2023).
- [30] B. Pettit, Z. Ákos, T. Vicsek, and D. Biro, Speed Determines Leadership and Leadership Determines Learning during Pigeon Flocking, *Current Biology* **25**, 3132 (2015).
- [31] D. Weihs, Energetic advantages of burst swimming of fish, *Journal of Theoretical Biology* **48**, 215 (1974).
- [32] R. Harpaz, G. Tkačik, and E. Schneidman, Discrete modes of social information processing predict individual behavior of fish in a group, *Proceedings of the National Academy of Sciences* **114**, 10149 (2017).
- [33] G. Li, I. Ashraf, B. François, D. Kolomenskiy, F. Lechenault, R. Godoy-Diana, and B. Thiria, Burst-and-coast swimmers optimize gait by adapting unique intrinsic cycle, *Communications Biology* **4**, 40 (2021).
- [34] J. E. Herbert-Read, A. S. I. Wade, I. W. Ramnarine, and C. C. Ioannou, Collective decision-making appears more egalitarian in populations where group fission costs are higher, *Biology Letters* **15**, 20190556 (2019).

- [35] T. Chen and C. Guestrin, XGBoost: A Scalable Tree Boosting System, in *Proceedings of the 22nd ACM SIGKDD International Conference on Knowledge Discovery and Data Mining*, KDD '16 (Association for Computing Machinery, New York, NY, USA, 2016) pp. 785–794.
- [36] H. E. A. MacGregor and C. C. Ioannou, Shoaling behaviour in response to turbidity in three-spined sticklebacks, *Ecology and Evolution* **13**, e10708 (2023).
- [37] S. V. Viscido, M. Miller, and D. S. Wetthey, The Dilemma of the Selfish Herd: The Search for a Realistic Movement Rule, *Journal of Theoretical Biology* **217**, 183 (2002).
- [38] L. J. Morrell, G. D. Ruxton, and R. James, Spatial positioning in the selfish herd, *Behavioral Ecology* **22**, 16 (2011).
- [39] J. Krause, The effect of 'Schreckstoff' on the shoaling behaviour of the minnow: A test of Hamilton's selfish herd theory, *Animal Behaviour* **45**, 1019 (1993).
- [40] A. De Vos and M. J. O'Riain, Sharks shape the geometry of a selfish seal herd: Experimental evidence from seal decoys, *Biology Letters* **6**, 48 (2010).
- [41] A. J. King, A. M. Wilson, S. D. Wilshin, J. Lowe, H. Haddadi, S. Hailes, and A. J. Morton, Selfish-herd behaviour of sheep under threat, *Current Biology* **22**, R561 (2012).
- [42] D. W. Sankey, R. F. Storms, R. J. Musters, T. W. Russell, C. K. Hemelrijk, and S. J. Portugal, Absence of "selfish herd" dynamics in bird flocks under threat, *Current Biology*, S0960982221006680 (2021).
- [43] T. L. Hammer, P. Bize, B. Gineste, J.-P. Robin, R. Groscolas, and V. A. Viblanc, Disentangling the "many-eyes", "dilution effect", "selfish herd", and "distracted prey" hypotheses in shaping alert and flight initiation distance in a colonial seabird, *Behavioural Processes* **210**, 104919 (2023).
- [44] R. A. Stein and J. J. Magnuson, Behavioral Response of Crayfish to a Fish Predator, *Ecology* **57**, 751 (1976).
- [45] M. Papadopoulou, H. Hildenbrandt, D. W. E. Sankey, S. J. Portugal, and C. K. Hemelrijk, Emergence of splits and collective turns in pigeon flocks under predation, *Royal Society Open Science* **9**, 211898 (2022).
- [46] E. Gimeno, V. Quera, F. S. Beltran, and R. Dolado, Differences in shoaling behavior in two species of freshwater fish (*Danio rerio* and *Hyphessobrycon herbertaxelrodi*), *Journal of Comparative Psychology* **130**, 358 (2016).
- [47] F. Romero-Ferrero, M. G. Bergomi, R. C. Hinz, F. J. H. Heras, and G. G. de Polavieja, Idtracker.ai: Tracking all individuals in small or large collectives of unmarked animals, *Nature Methods* **16**, 179 (2019).

## ACKNOWLEDGMENTS

We acknowledge financial support from projects PID2022-137505NB-C21 and PID2022-137505NB-C22 funded by MICIU/AEI/10.13039/501100011033, and by "ERDF: A way of making Europe". We thank F. Mazzanti, E. Romero and D. Bierbach for helpful discussions.

## AUTHOR CONTRIBUTIONS

A.P., F.S.B., R.D., M.C.M., R.P.-S. designed the study. E.G. acquired and processed the empirical data. A.P. analyzed the empirical data. A.P. and R.P.-S. developed the machine learning tool. A.P., M.C.M., C.C.I., R.P.-S. analyzed the results. A.P., C.C.I., R.P.-S. wrote the paper. All authors commented on the manuscript.

## COMPETING INTERESTS

The authors declare no competing interests.

## **SUPPLEMENTARY INFORMATION**

Video S1. Rendering of the movement of fish overlaid with the digitized trajectories. We show habituated and non-habituated individuals in blue and red, respectively.

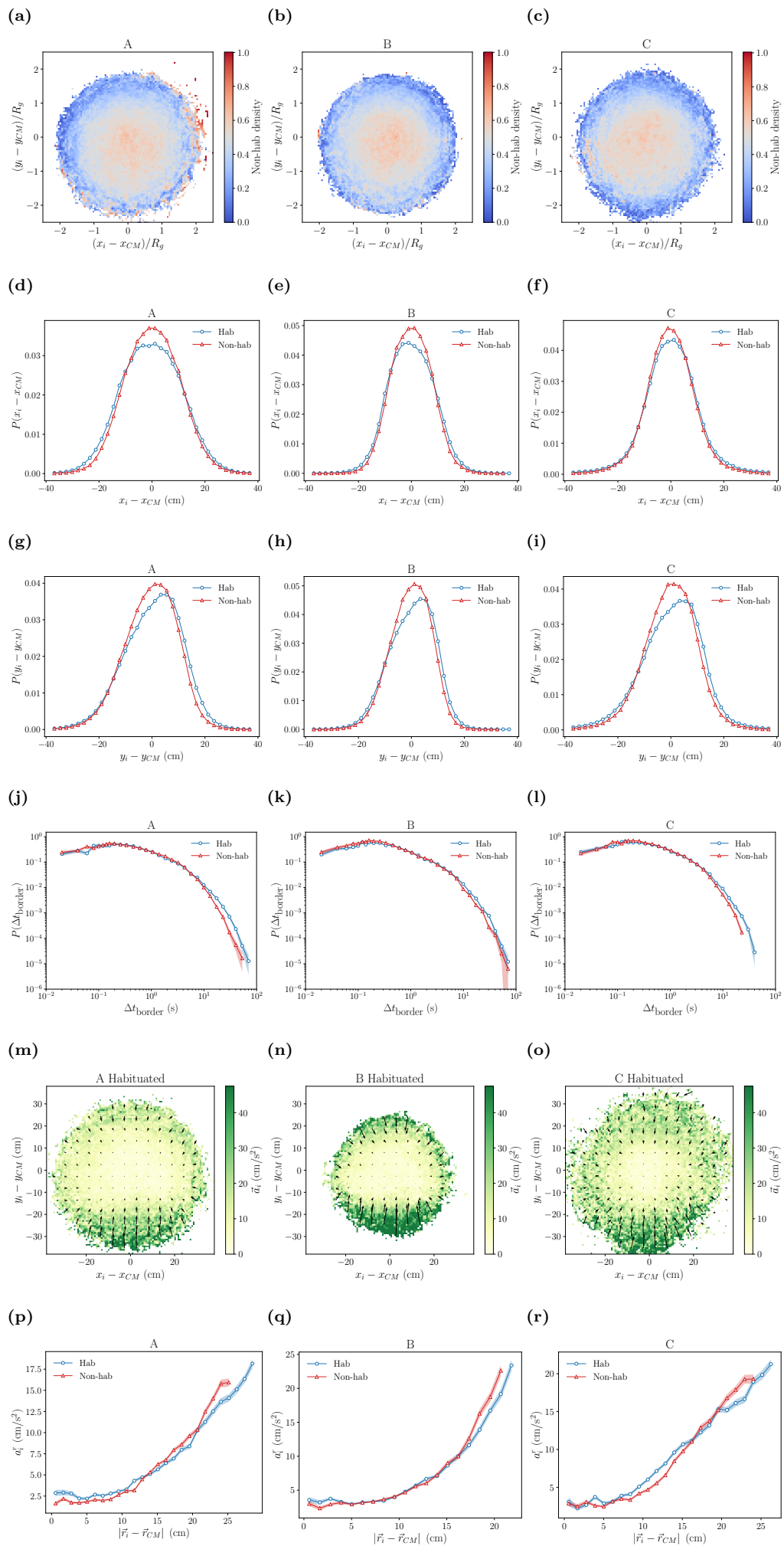


FIG. S1. Group-level spatial interactions (see Fig. 1) for different series.

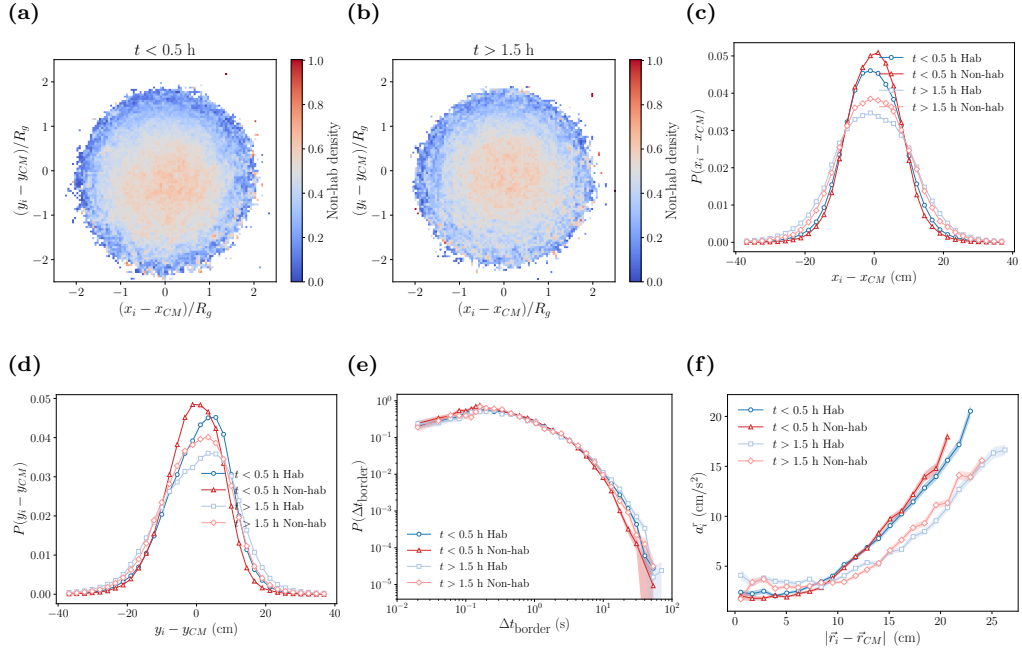


FIG. S2. Temporal evolution of group-level spatial interactions (see Fig. 1). Results are compared for the first half-hour and last half-hour of the experiment.

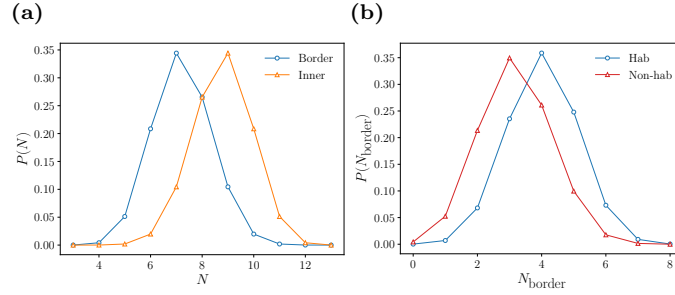


FIG. S3. PDF of (a) the number of individuals  $N$  at the border and at the inner part of the group and (b) the number of individuals at the border  $N_{\text{border}}$  for habituated and non-habituated individuals.

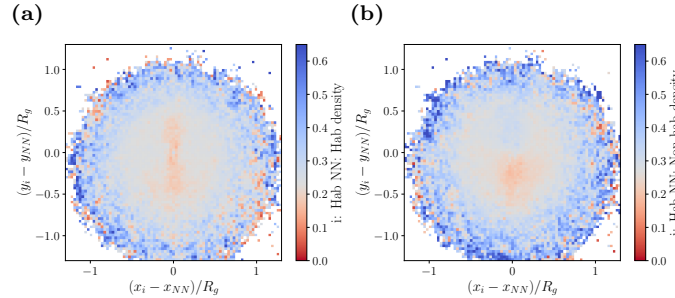


FIG. S4. (a) and (b) Density of habituated individuals  $i$  with (a) habituated and (b) non-habituated nearest-neighbors  $NN$  depending on the relative position of the individual with the nearest neighbor.



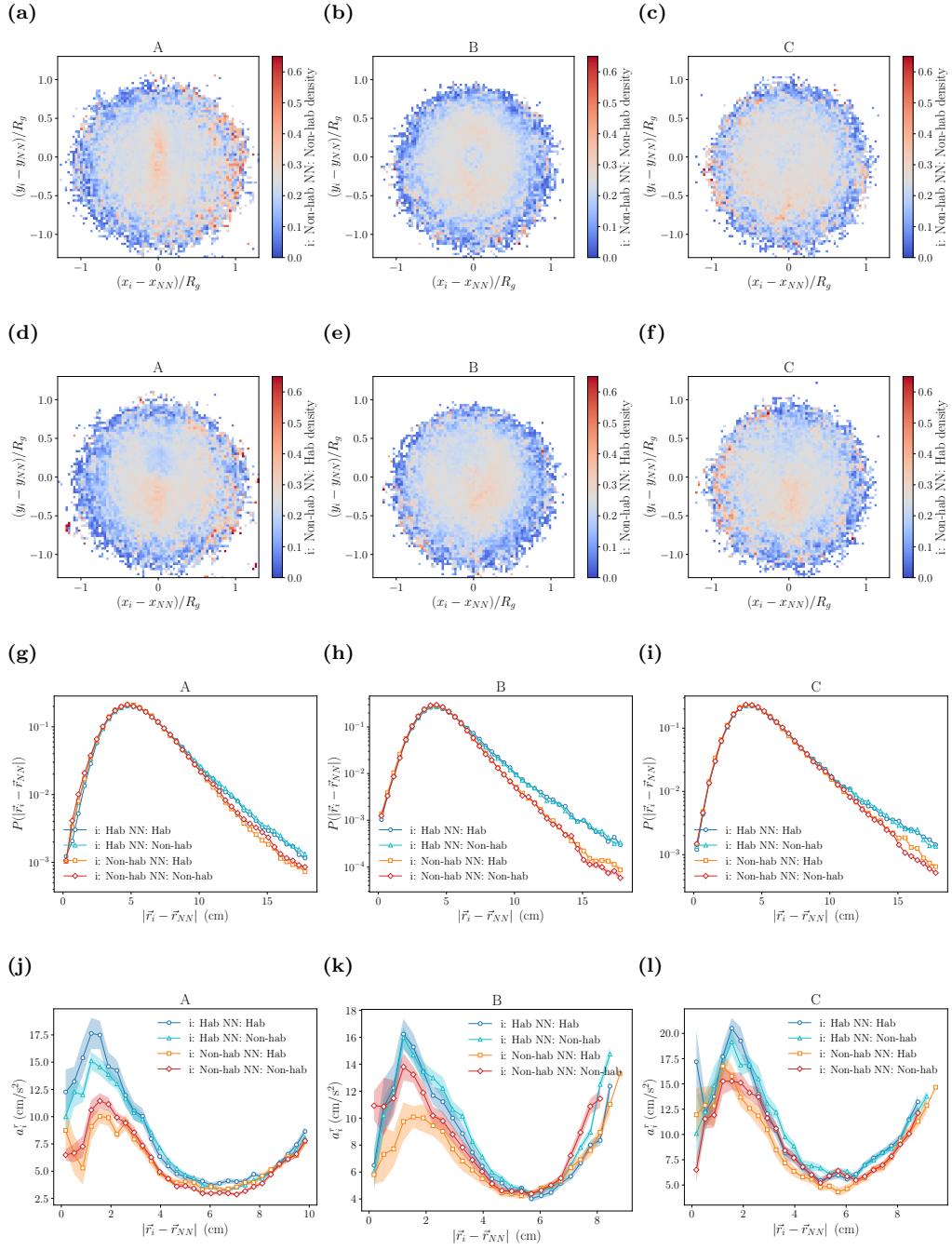


FIG. S5. Local-level spatial interactions (see Fig. 2) for different series.

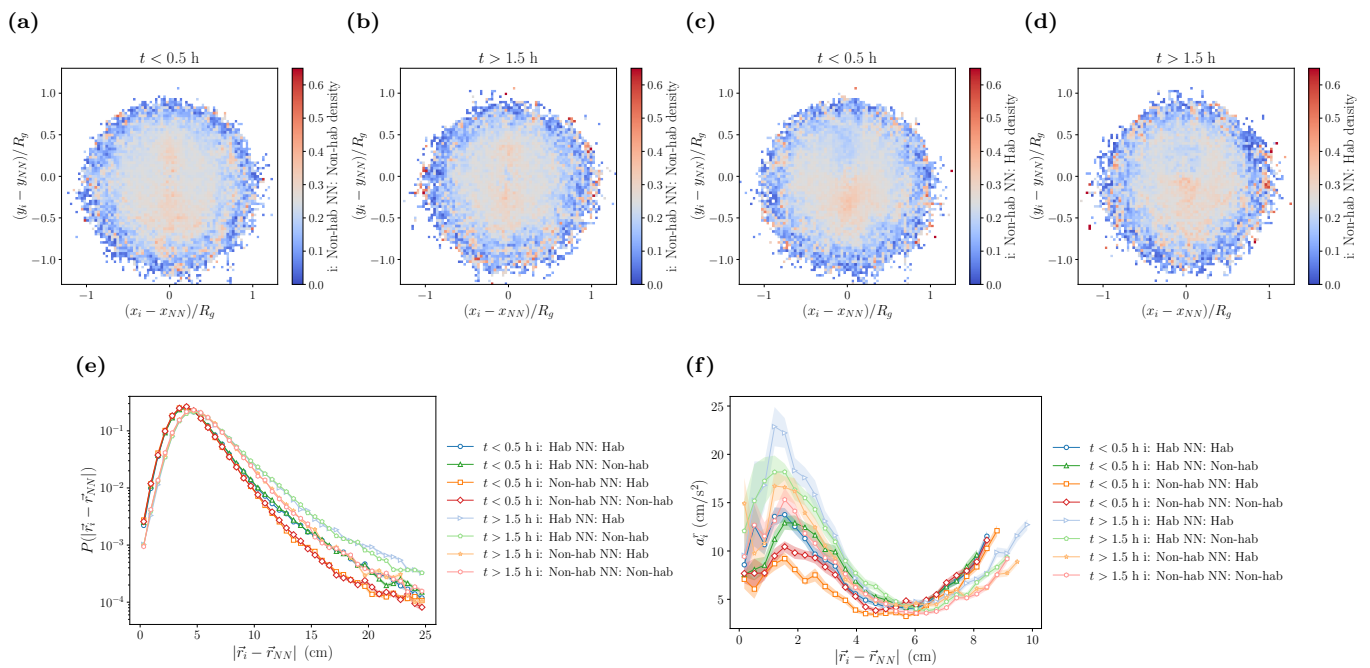


FIG. S6. Temporal evolution of local-level spatial interactions (see Fig. 2).

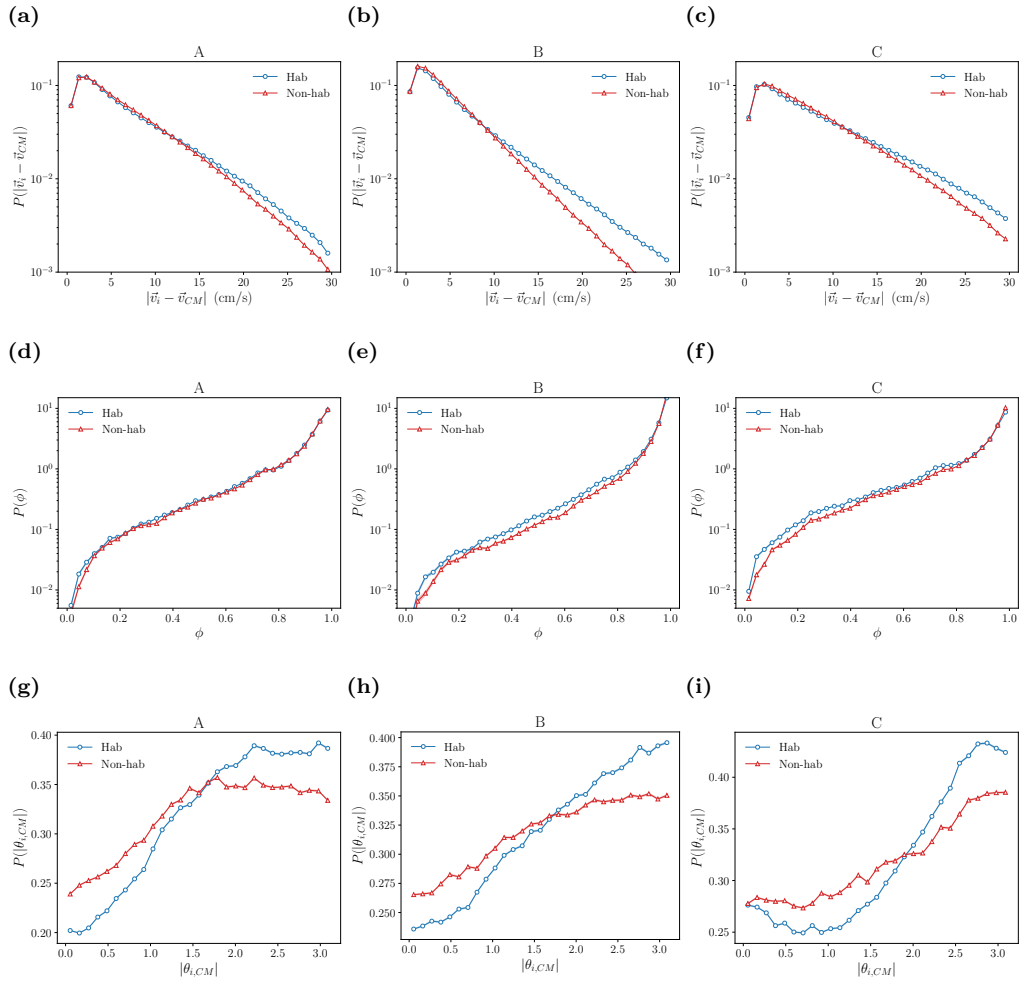


FIG. S7. Group-level coordination (see Fig. 3) for different series.

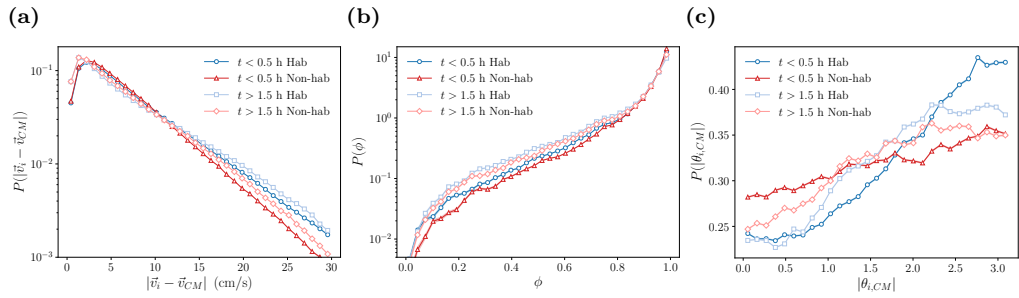


FIG. S8. Temporal evolution of group-level coordination (see Fig. 3).

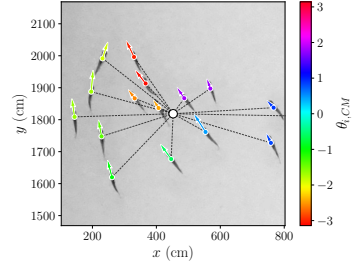


FIG. S9. Sample of the positions of individuals  $\vec{r}_i$  color-coded by the individuals orientation relative to the center of mass (CM),  $\theta_{i,CM}$ . The white circle corresponds to the CM.

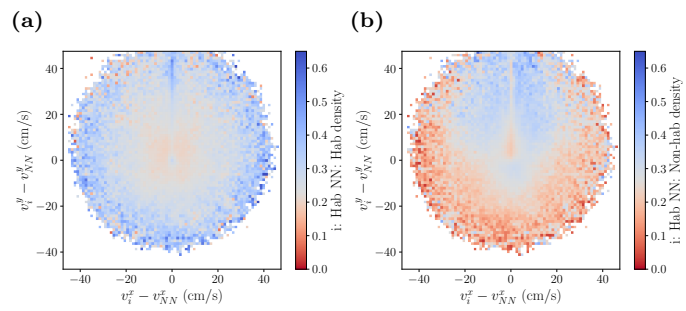


FIG. S10. (a) and (b) Density of habituated individuals  $i$  with (a) habituated and (b) non-habituated nearest-neighbors  $NN$  depending on the relative velocity of the individual with the nearest neighbor.

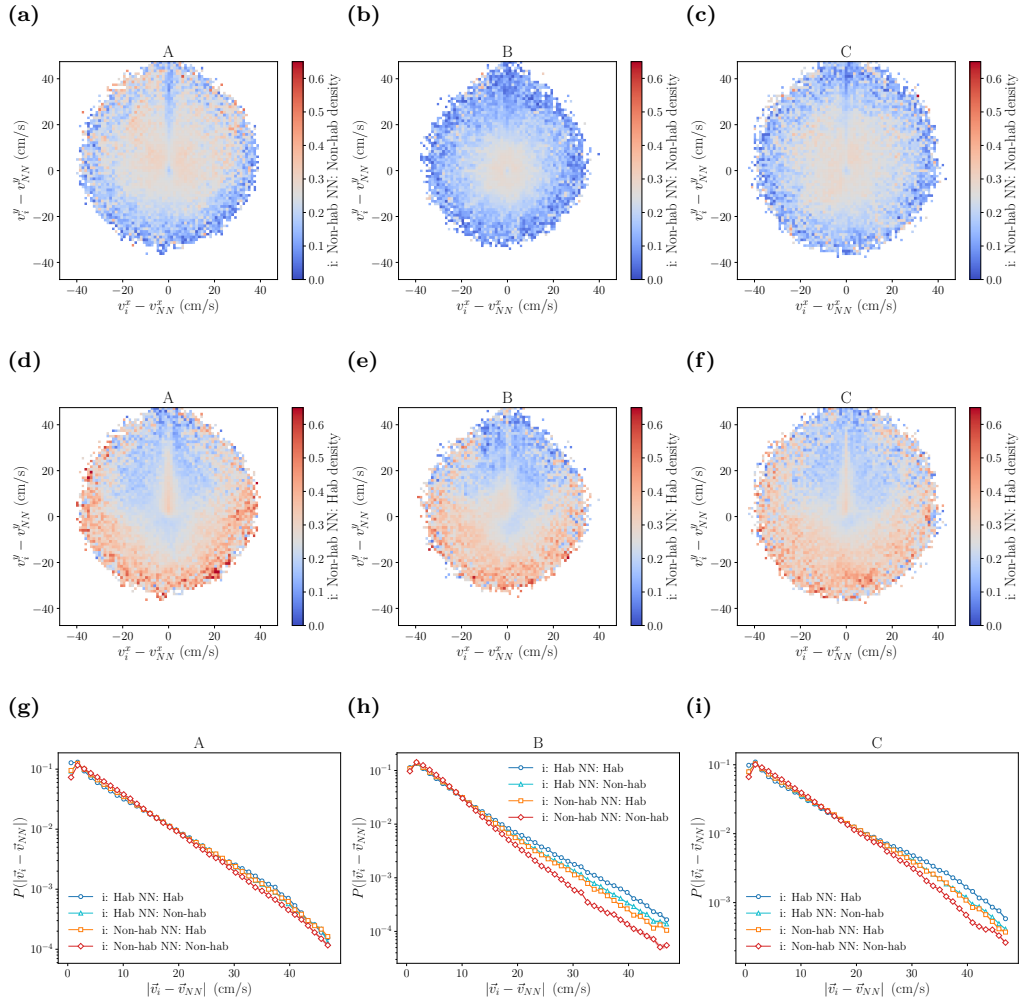


FIG. S11. Local-level coordination (see Fig. 4) for different series.

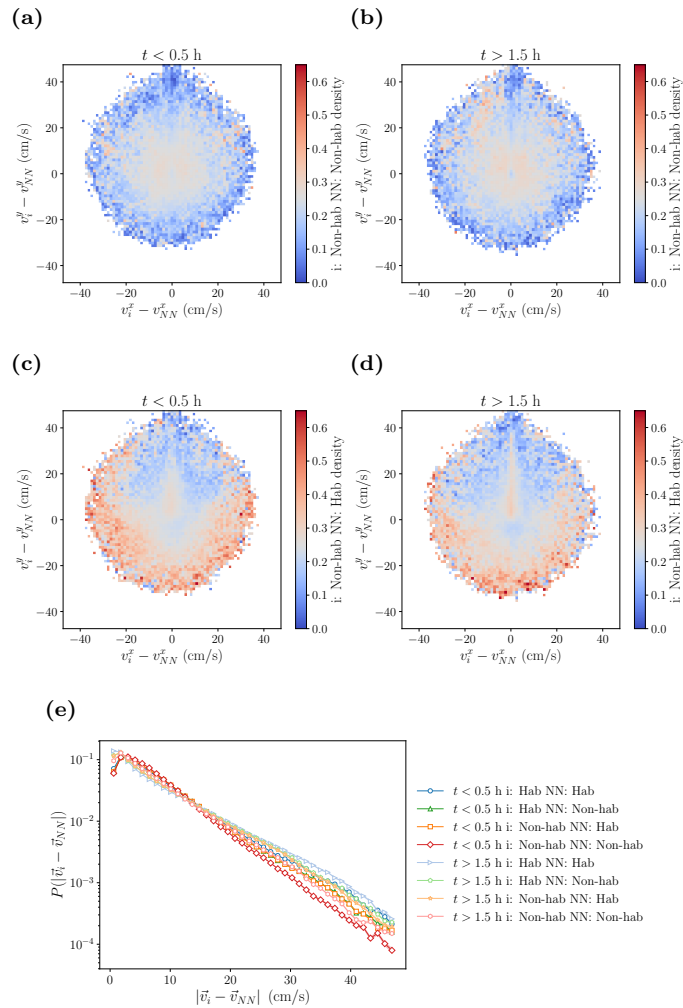


FIG. S12. Temporal evolution of local-level coordination (see Fig. 4).

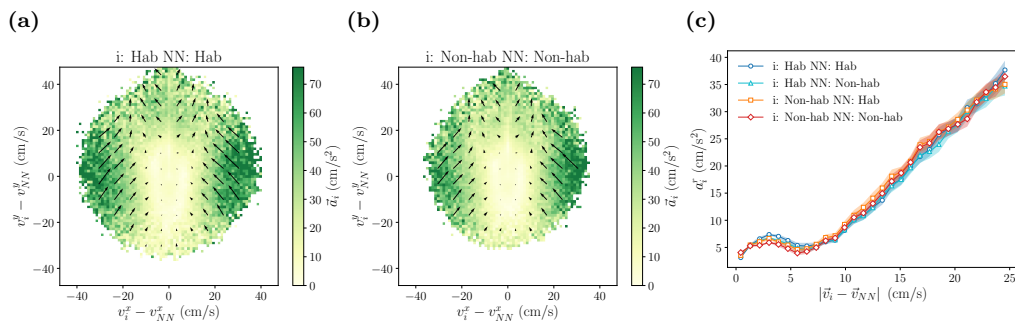


FIG. S13. Local-level alignment force map. (a) and (b) Average acceleration (alignment force map) of individual  $i$  depending on the relative velocity with the nearest neighbor,  $\vec{v}_i - \vec{v}_{NN}$ , between (a) habituated and (b) non-habituated individuals, and (c) average projection of the acceleration in the radial direction of the alignment force map,  $|\vec{v}_i - \vec{v}_{NN}|$ .

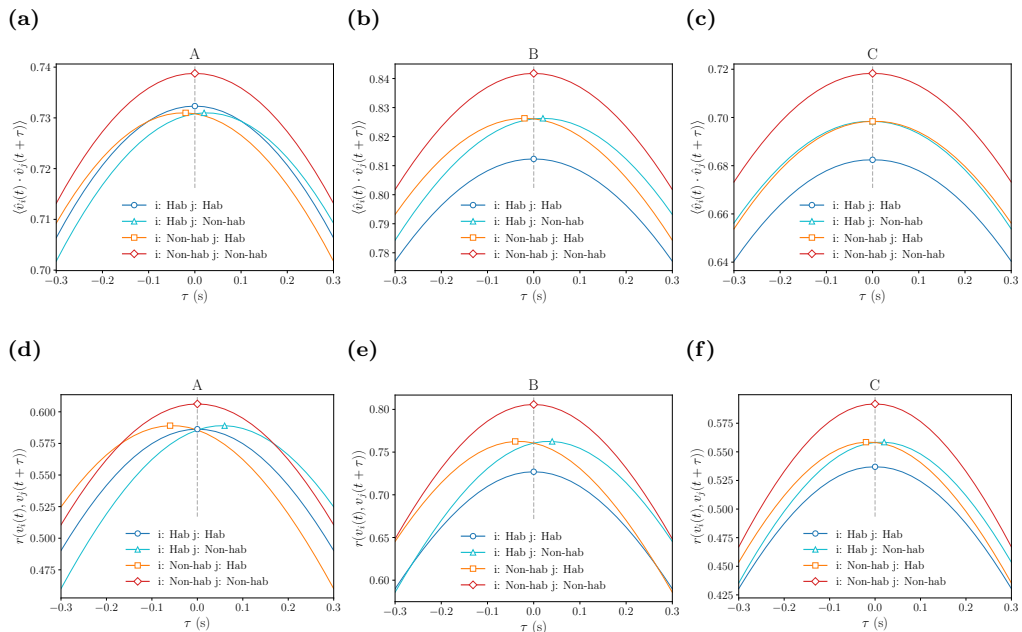


FIG. S14. Leader-follower relationships (see Fig. 5) for different series.

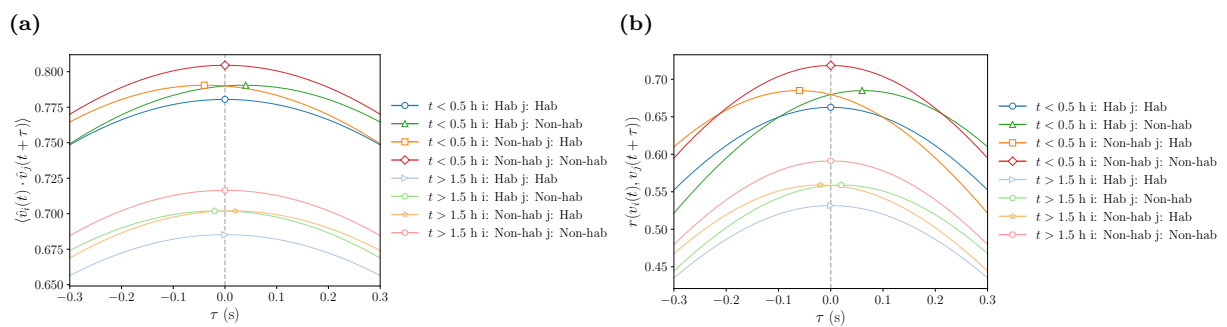


FIG. S15. Temporal evolution of leader-follower relationships (see Fig. 5).

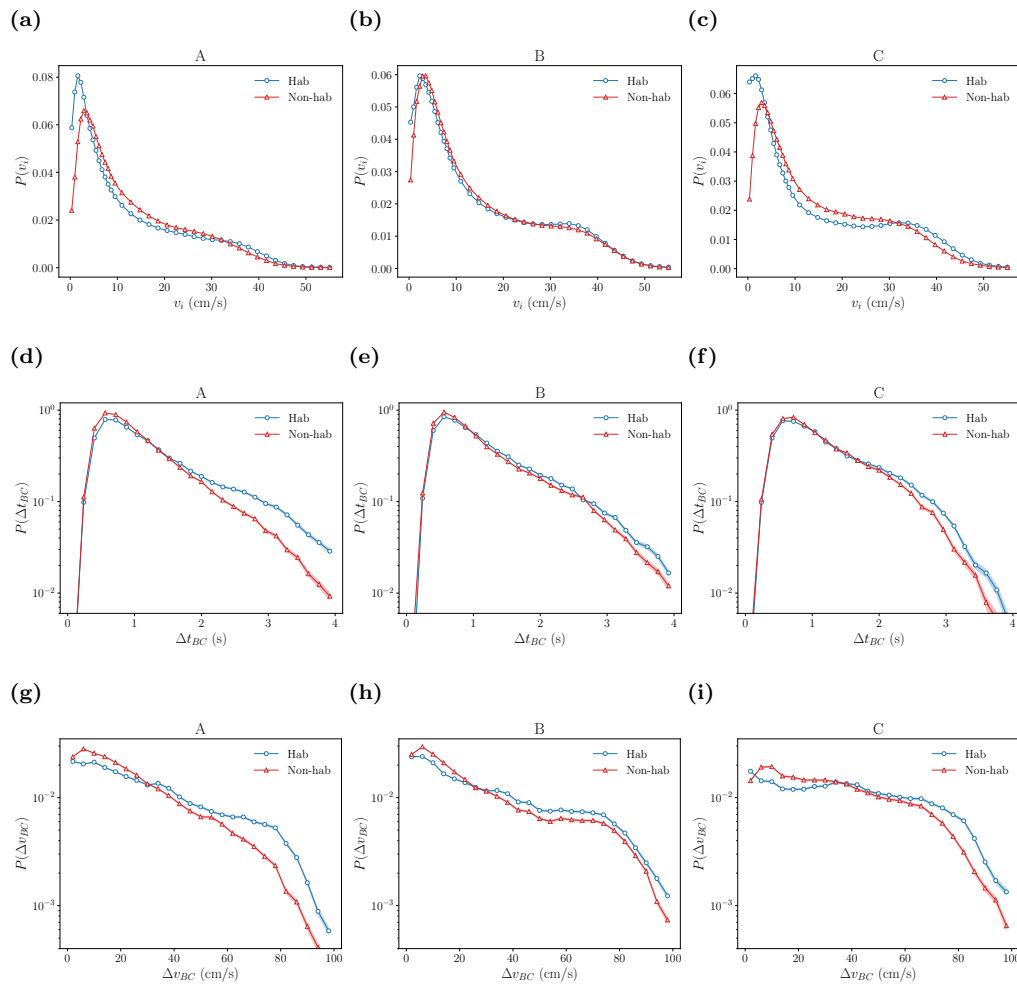


FIG. S16. Burst-and-coast dynamics (see Fig. 6) for different series.

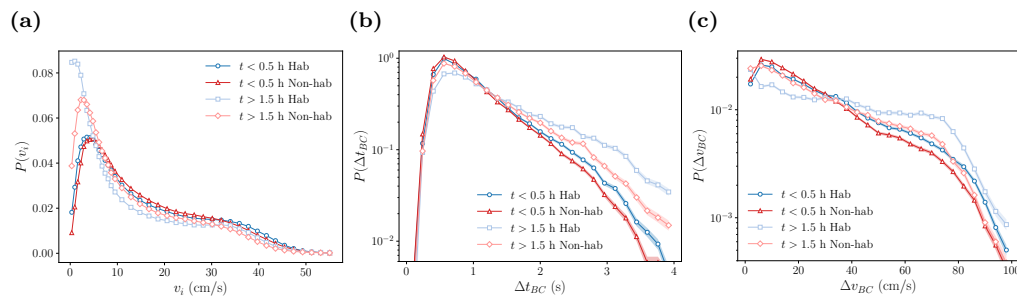


FIG. S17. Temporal evolution of burst-and-coast dynamics (see Fig. 6)



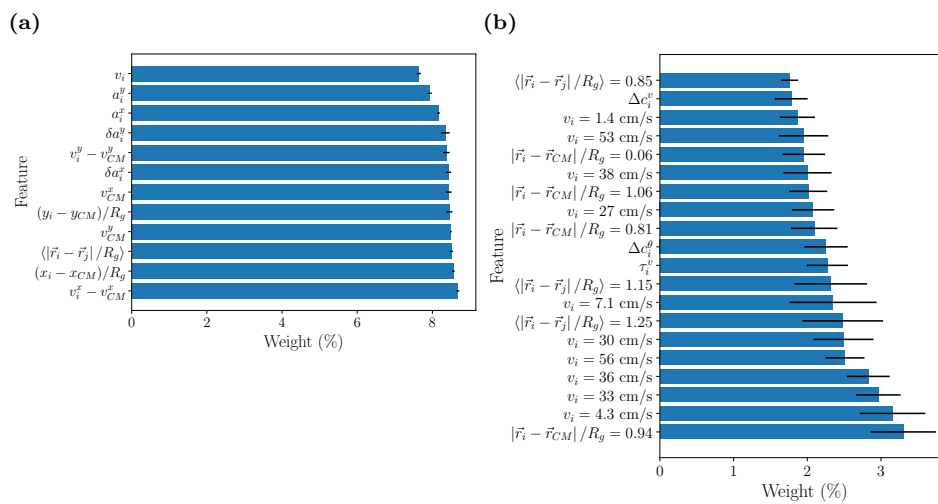


FIG. S18. Feature weights for (a) the instantaneous and (b) the temporal window machine learning tools. They are averaged across (a) 4 folds and (b) 30 folds of the cross-validation. In (b), we only show the 20 highest weight features.

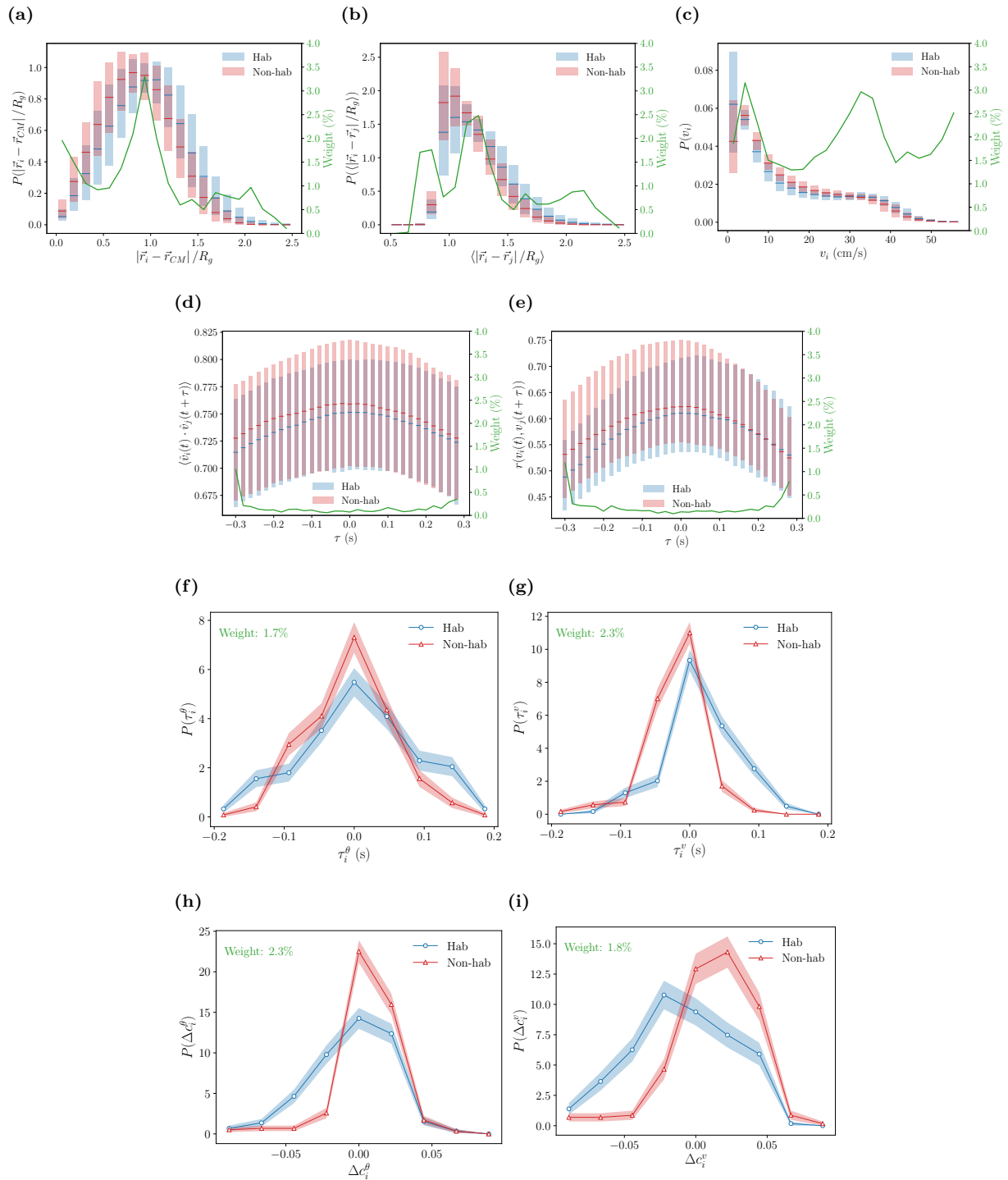


FIG. S19. Features of the temporal window machine learning tool. (a) Histogram of the normalized distance to the center of mass  $|\vec{r}_i - \vec{r}_{CM}|/R_g$ , (b) histogram of the average normalized distance to other individuals  $\langle |\vec{r}_i - \vec{r}_j|/R_g \rangle$ , (c) histogram of the speed  $v_i$ , (d)-(e) leader-follower correlations averaged across other individuals  $j$  (d) in the orientation  $\langle \hat{v}_i(t) \cdot \hat{v}_j(t + \tau) \rangle$  and (e) in the speed  $r(v_i(t), v_j(t + \tau))$ , (f)-(g) PDF of the delay of the maximum correlations in (f) the orientation  $\tau_i^\theta$  and (g) the speed  $\tau_i^v$  and (h)-(i) relative difference of the maximum correlation value with respect to the group in (h) the orientation  $\Delta c_i^\theta$  and (i) the speed  $\Delta c_i^v$ . In (a)-(e), box plots indicate the first, second, and third quartiles of the function for individuals within the subgroups. In green we show the feature weights of the machine learning algorithm, averaged across 30 folds of cross-validation.